High-temperature Impedance and Dielectric Studies of $Ni_{0.5}Zn_{0.5}WO_4$ Micro Stone Prepared Via Solid-state Route

Subrata Karmakar[1, a)] and Dhrubananda Behera[1]

[1]Department of Physics & Astronomy, National Institute of Technology Rourkela, Rourkela-769008, Odisha, India.
[a)] *Corresponding author: 516ph1010@nitrkl.ac.in, dbehera@nitrkl.ac.in*

Abstract

The $Ni_{0.5}Zn_{0.5}WO_4$ microtone was prepared via conventional solid-state synthesis techniques and its phase formation with monoclinic structure (space group- P2/c) was investigated with a view to understand its structural, morphological and dielectric properties. The phase formation and average particle size (31.38 μm) were ascertained by X-ray Diffractometry (XRD) and Field emission Scanning Electron Microscope (FESEM) techniques respectively. The real and imaginary impedance Z', Z'', dielectric constant (ϵ_r), loss (δ) and ac conductivity (σ_{ac}) was measured in the frequency range 100Hz-1MHz with high-temperature evolution (200° c-460° c).The dominancy of electrode ceramic effect and Non-Debye type dipolar relaxation was observed with high temperature evolution above 200^0c.The dielectric constant and loses was enhances with increase of temperature and ac conductivity was fitted with well-known Jonscher power law with dc activation energy 0.834 eV.

Keywords: Nickel-zinc tungstate, impedance spectra, dielectric constant and loss, ac conductivity, dc activation energy

1. Introduction

Nowadays, the transition metal tungstate MWO_4 (Ni, Zn, Mg, Co) have been attracted much attention due to their structural, magnetic and optical properties [1, 2]. Among them, $NiWO_4$ and $ZnWO_4$ are technologically promising materials for their versatile applications like humidity sensors, microwave, photoluminescence, acoustic, optical fibers, phase-change optical recording, magnetic properties and catalysis etc. [3, 6]. The dielectric and thermo-physical properties of $NiWO_4$ and $ZnWO_4$ were investigated by various researchers [7] but the electrical transport properties of $Ni_{0.5}Zn_{0.5}WO_4$ are still unreported. The unique combination of physical, chemical properties (with regard to electronic and molecular versatility, stability and reactivity) and identical ionic radius of Ni (83 pm) and Zn (88 pm) motivated us to characterize the modified structural and dielectric properties of $Ni_{0.5}Zn_{0.5}WO_4$ for its explored application in high temperature.

In this present work, we prepared $Ni_{0.5}Zn_{0.5}WO_4$ Micro particles Via conventional solid-state

route and made an attempt to study the high temperature dielectrics and ac conductivity analysis. Impedance spectroscopy estimations over a reasonable frequency range can permit the clarification of the contributing impacts of the bulk counterpart and grain boundaries to the entire conductivity of the sample.

2. Experimental Details

2.1 Materials used and synthesis process

The $Ni_{0.5}Zn_{0.5}WO_4$ micro stone were prepared by solid-state synthesis technique taking NiO (99.99%), ZnO (99.99%) and WO_3 (99.99%) as primary raw reagent with their stoichiometric ratios (0.5:0.5:1). All chemicals were mixed properly, grind well for 2 hours and calcined at 900^0c for 12 hours. The obtained powder again grinds well to make pallet and sintered at 900^0c for 6 hours. The solid-state synthesis processes are portrayed below-

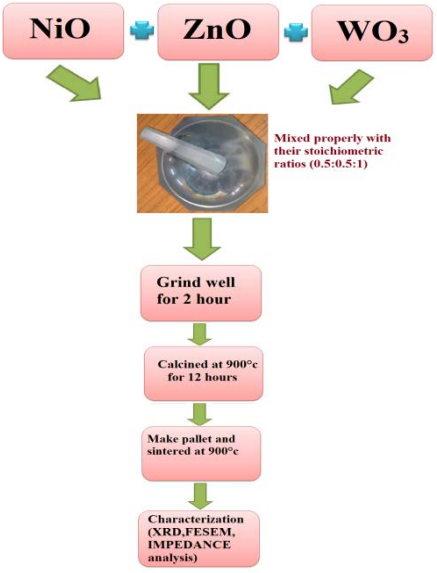

Scheme.1: Schematic flow-chart of synthesis of $Ni_{0.5}Zn_{0.5}WO_4$ micro particles.

3. Result and Discussion

3.1 Structural & Morphological Analysis

The as-prepared samples were characterized by X-Ray diffractometer techniques (X-Pert, PANalytical, PW 3040/00, Netherlands) using Co-Kα source in the 2Θ range of 20° to 80° is shown in [Fig.1A]. The XRD refinement reveals the monoclinic wolframite-type structure of $Ni_{0.5}Zn_{0.5}WO_4$ with P2/c space group and C_{2h} point group symmetry lattice parameter $a = 4.6525Å,\ b = 5.702Å, c = 4.8923Å$ and $\beta=90^0$ respectively [8, 9]. The surface morphology was characterized by Field emission Scanning Electron Microscope (Nova NanoSEM/FEI with resolution 1.4 nm @ 1 kV). The FESEM micrographs of $Ni_{0.5}Zn_{0.5}WO_4$

powder samples are represented in [Fig.1A inset] which exhibits its stone-like crystal growth in μm range and the average particle sizes were determined around 31.38 μm. The EDS spectra displayed the presence of elemental compound Ni, Zn, W and O with their normalized weight and atomic percentages are shown in [Fig.1B].

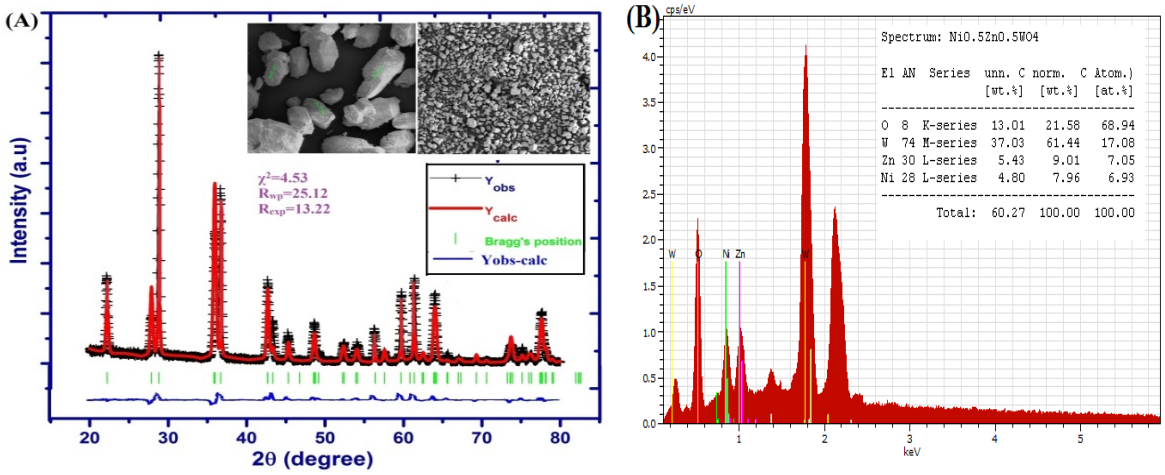

Fig.1: The Xrd pattern (A) and EDAX spectra (B) of as-synthesized $Ni_{0.5}Zn_{0.5}WO_4$ micro stone.

3.2 Impedance Analysis

The frequency dispersive real and imaginary impedance spectra are carried out by Hioki impedance analyser IM3570 between 100 Hz-1 MHz at the different temperature from 200°c-460°c are shown in [Fig.2 A&B]. The frequency independent dc conductivity plateau strengthens itself with high-temperature evolution and frequency dependent ac conductivity curtailed gradually. The similar identical trends were observed from the ac conductivity plot. The Z'' was also decreased monotonically with an increase of frequency and merged together with a higher frequency which indicates the weak relaxation in low temperatures. This arises due to the freezing of dipoles and consequently, the small values of dielectric constant and loss were observed at low temperatures. The cole-cole plot ($Z' - Z''$) of impedance assures the presence of the grain, grain boundary and electrode interface contribution and modeled in terms of their equivalent circuit which was displayed in [Fig.2 C&D]. The complex impedance can be expressed as,

$Z^* = Z' - iZ'' = \frac{1}{R_g^{-1}+j\omega C_g} + \frac{1}{R_{gb}^{-1}+j\omega C_{gb}} + \frac{1}{R_{el}^{-1}+j\omega C_{el}}$, where real ($Z' = Zcos\theta$) and imaginary ($Z'' = Zsin\theta$) impedance can be represented as [10],

$$Z' = \frac{R_g}{1+(\omega R_g C_g)^2} + \frac{R_{gb}}{1+(\omega R_{gb} C_{gb})^2} + \frac{R_{el}}{1+(\omega R_{el} C_{el})^2} \ldots (1)$$

$$Z'' = R_g\left[\frac{\omega R_g C_g}{1+(\omega R_g C_g)^2}\right] + R_{gb}\left[\frac{\omega R_{gb} C_{gb}}{1+(\omega R_{gb} C_{gb})^2}\right] + R_{el}\left[\frac{\omega R_{el} C_{el}}{1+(\omega R_{el} C_{el})^2}\right] \quad \ldots (2)$$

Where ω is the angular frequency and R_g, R_{gb}, R_{el} and C_g, C_{gb}, C_{el} is grain, grain boundary, electrode interfaces resistance and capacitance respectively. The electrode ceramic interface contribution for surface charge polarizations plays an important role in the cole-cole plot in high temperature and it dominates the grain and grain boundary contribution above 200°c. The unique relaxation processes were modeled with R(QR)(QR)(CR) circuits by ZSimpWin software and the extracted parameters confirm the prevalence of electrode ceramic effect. The constant phase elements (CPE) are related to the capacitance and resistance value of grain, grain boundary and can be expressed as [11],

$C = (R^{1-\alpha}.Q)^{\frac{1}{\alpha}} \ldots$ (3)

The value of α is unity for the pure capacitor and zero for the pure resistor.

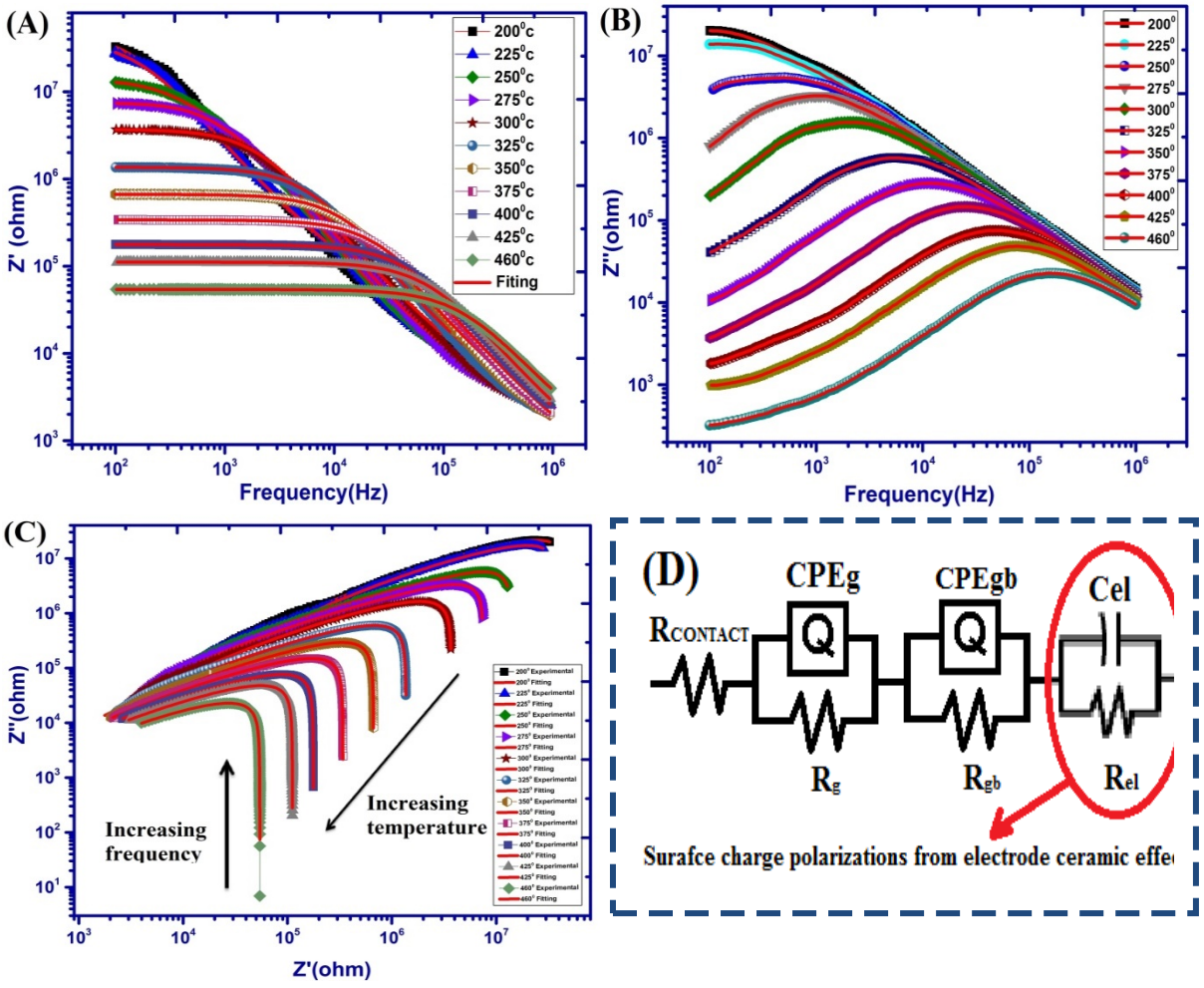

Fig.2: The frequency dependence real and imaginary impedance (A & B) and Cole-Cole plot (C) (Z' vs. Z'') of impedance at a different temperature.

3.3 Dielectric and ac Conductivity Analysis

The dielectric constant (ϵ_r) of the as-prepared samples was calculated from the plate capacitance (C_p) using the relation, $\epsilon_r = \frac{C_p d}{\epsilon_0 A}$ where C_p is the palate capacitance and d, A are

the thickness and area of the pallet. The dielectric constant lessened with the increase of the frequency of the applied field at any particular temperature and shown in [Fig.3A]. In low-frequency regime, dielectric constant arises due to combinations of several kinds of polarizations viz. deformational (ionic, electronic) as well as relaxation (interfacial and orientational). As soon as the frequency starts increasing, the electric dipoles unable to follow the frequency of the applied field and leads the diminish of orientational polarization. At high frequency, the dielectric constant reaches a stationary value due to interfacial polarization. In low temperature, the dipole cannot orient themselves due to less thermal excitation and lessened the dielectric constant at any particular frequency. The orientations of dipoles are facilitated by thermal movement at high temperature and enhance the electrical permittivity. The dielectric loss [Fig.3A inset] also followed similar trends like permittivity [12].

The ac conductivity of nickel-zinc tungstate micro-stone was determined using the following expressions; $\sigma_{ac} = \frac{d}{A}\frac{Z\prime}{Z\prime^2+Z\prime\prime^2}$. The total ac conductivity [Fig.3B] possesses two regions, (i) frequency dependent ac conductivity (ii) frequency independent dc conductivity which has been fitted by the acclaimed Jonscher power law, [13]

$$\sigma_t(\omega) = \sigma_{dc} + B\omega^n \ldots (4)$$

Where $\sigma_t(\omega)$ is the total ac conductivity and n is the frequency exponent. The variation of dc conductivity with inverse absolute temperature are shown in [Fig.3C] and it exhibits a linear response which was elucidated by a thermally activated transport of Arrhenius type equation which was governed by the relation below [14],

$$\sigma_{dc}T = \sigma_0 \exp(-E_a/k_BT) \ldots\ldots (5)$$

where σ_0, E_a and k_B are the pre-exponential factors, dc activation energy of mobile charge carriers and Boltzmann constant respectively. The dc activation energy for conduction processes was estimated 0.834 eV from the slope of the straight line.

The variation of frequency exponent n with temperature [Fig.3D] also suggests the possible reasons for the conduction mechanism. Hence, it was observed from the graph that the frequency exponent was increases gradually with temperature evolution and saturates. Thus, this result recommends that the conductivity mechanism can be manifested by non-overlapping small polaron tunnelling (NSPT) concept and the parameter n is evaluated as follows [15],

$$n = 1 - \frac{4}{\left[Ln\left(\frac{1}{\omega\zeta_0}\right) - \frac{\omega_h}{k_BT}\right]}$$

where, ζ_0 and ω_h denotes the characteristics relaxation time and polaron hopping energy.

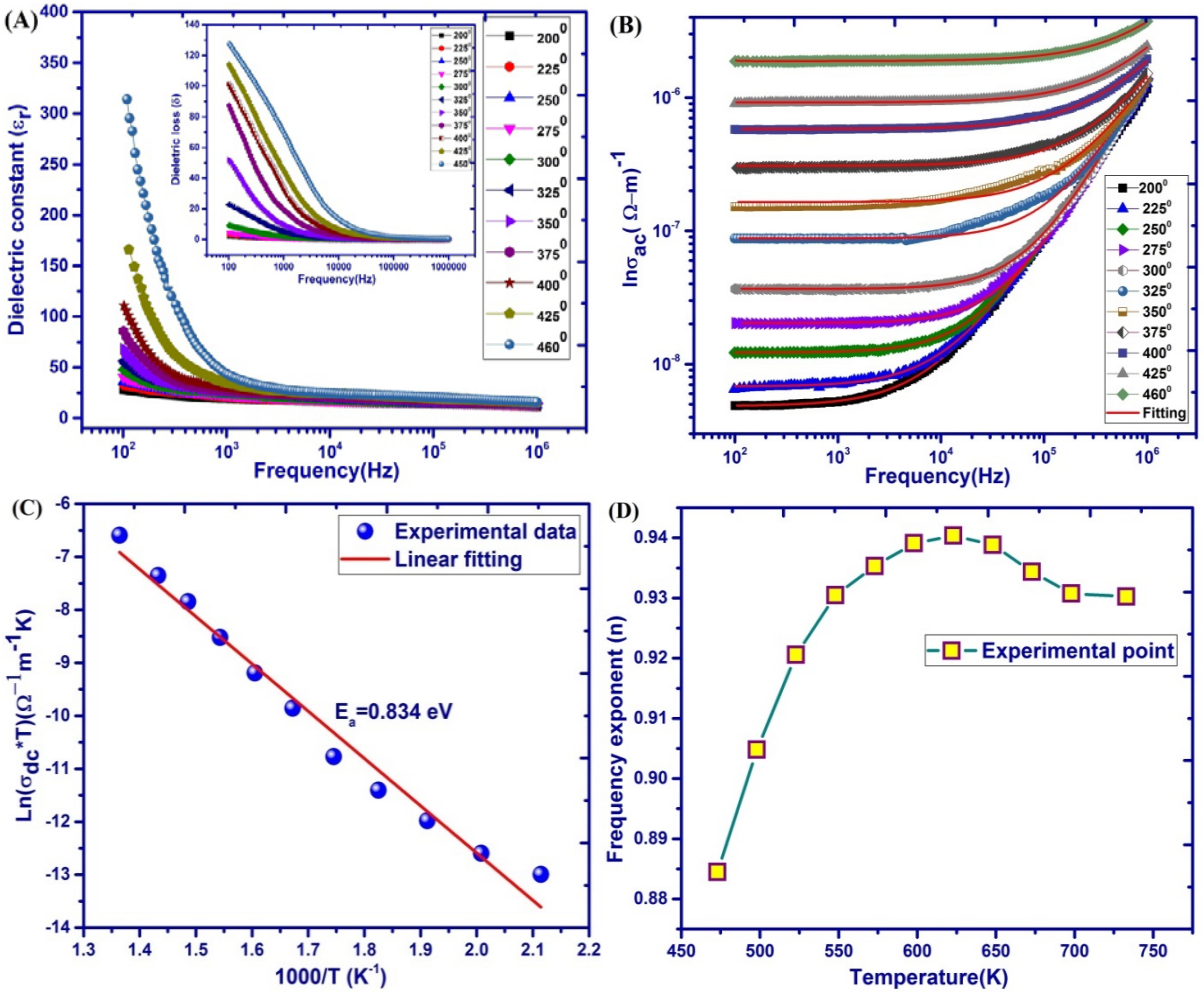

Fig.3: The dielectric constant (ϵ_r), loss (δ) (A), ac conductivity (B) vs. frequency, dc activation energy (C) and the variation of frequency exponent (D) at the different temperature

4. Conclusion

The $Ni_{0.5}Zn_{0.5}WO_4$ micro stone was synthesized via solid-state synthesis route and its phase formation and structural morphology were characterized by XRD and FESEM techniques. The intra and inter-grain contribution and dominancy of electrode ceramic surface charge polarizations were distinguished from a cole-cole plot of impedance spectra. The decaying nature of dielectric permitivity and loss with frequency dispersion was observed and it recommednds the Maxwell-wagner type surface charge polraizations.The ac conductivity was fitted with the well-known Jonscher single power law and the dc activation energy (0.834 eV) was estimated from the slope. The growing nature of frequency exponent with absolute temperature suggests the non-overlapping small polaron tunneling mechanism in conduction processes.

5. Acknowledgements

The authors are thankful to all faculty members and Ph.D scholar of NIT Rourkela for providing necessary laboratory facilities whenever required.

6. References

[1] Wang BG, Shi EW, Zhong WZ, Yin ZW, J Inorg Mater. **13** (1998), pp 648–654.
[2] H. Grassmann, H.G. Moser, J. Lumin. **33** (1985), pp 109–113.
[3] G. Huang and Y. Zhu, Mater. Sci. Eng. B **139** (2007), p 201.
[4] G. Huang, C. Zhang, and Y. Zhu, J. Alloys Compd. **432** (2007), p 269.
[5] F. Yang, C. Tu, H. Wang, Y. Wei, Z. You, G. Jia, J. Li, Z. Zhu, X. Lu, and Y. Wang, Opt. Mater.**29** (2007), p 1861.
[6] J. Lin, J. Lin, and Y. Zhu, Inorg. Chem. **46** (2007), p 8372.
[7] C. P. Landee and E.F. Westrum, Jr. Journal of Chemical Thermodynamics. **8** (1976), pp 471-491.
[8] A. Mekap, P. R. Das, R. N. P. Choudhary, Journal of Electronic Materials. **43** (2014), pp 3527–3533.
[9] R. O. KILLING, Acta Cryst. **10** (1975), p 209.
[10] D.C. Sinclair, Bol. Soc. Esp. Cerem.Vidrio. **34** (1995), pp 55–65.
[11] J.H. Joshi, D.K. Kanchan, M.J. Joshi, H.O. Jethva, K.D. Parikh, Materials Research Bull. **93** (2017), pp 63–73.
[12] A.Gantassi, H.Essaidi, Z.Ben Hamed, D.Gherouel, K.Boubaker, A.Colantoni, D.Monarca, F.Kouki, M.Amlouk, T.Manoubi, Journal of Crystal Growth. **413** (2015), pp 51-60.
[13] N. Ortega, Ashok Kumar, P. Bhattacharya, S.B.Majumder, R.S. Katiyar, Phys. Rev. B 77 (2008), p 014111.
[14] S. Nasri, A. L. Ben Hafsia, M. Tabellout and M. Megdiche, RSC Adv., **6** (2016), p 76659.
[15] M. Dult, R. S. Kundu, S. Murugavel, R. Punia and N. Kishore, Phys. B, **452** (2014),p 102.